Solidified Liquid Metal with Regulated Plasticity for Channel-Free Construction of 3D Structured Flexible Electronics

Guoqiang Li
Harbin Institute of Technology (Shenzhen)
Mingyang Zhang
Harbin Institute of Technology (Shenzhen)
Sanhu Liu
Harbin Institute of Technology
Man Yuan
Harbin Institute of Technology (Shenzhen)
Junjie Wu
Harbin Institute of Technology (Shenzhen)
Mei Yu
Chinese Academy of Sciences
Zhiwu Xu
Harbin Institute of Technology
Jinhong Guo
University of Electronic Science and Technology of China
Li Guanglin
Shenzhen Institutes of Advanced Technology
Zhiyuan Liu
Shenzhen Institute of Advanced Technology, Chinese Academy of Sciences
Xing Ma (maxing@hit.edu.cn)
Harbin Institute of Technology (Shenzhen) https://orcid.org/0000-0002-2248-4806

Article

Keywords: Gallium Alloy Based Liquid Metals, Soft and Stretchable Electronics, 3D Structured Circuits, Microchannels

Posted Date: June 14th, 2021

DOI: https://doi.org/10.21203/rs.3.rs-554970/v1

Version of Record: A version of this preprint was published at Nature Electronics on January 30th, 2023.
See the published version at https://doi.org/10.1038/s41928-022-00914-8.

Abstract

Gallium alloy based liquid metals (LMs) have shown great promise for soft and stretchable electronics in virtue of intrinsic fluidity and metallic conductivity. However, it has been a challenge by using LM to construct 3D structured circuits which are crucial for building flexible electronics with high integration. Hereby, taking advantage of the solid-liquid phase transition and plastic deformation of a Ga-10In LM alloy, we propose a novel strategy to fabricate LM based flexible electronic devices, in particular comprised of 3D circuits, without the need to pre-fabricate microchannels. We demonstrate applications including 3D interconnect arches for the integration of a multi-channel LED array, a 3D structured wearable sensor and a multilayer flexible circuit board for monitoring of finger movement. The current work provides a facile strategy for constructing LM based flexible electronics, which is of particular interest for building highly integrated electronics of hierarchical structure involving complicated 3D circuits.

Introduction

Soft and stretchable conductors play a crucial role in the designs of next-generation flexible electronic devices with high strain tolerance, e.g., in human-machine interfaces[1-4], soft robotics[5], and wearable healthcare monitoring devices[6-9]. Being basic building blocks of flexible electronics, stretchable conductors have received much attention and great efforts have been devoted to improve their design and manufacturing process, which leads to numerous innovations in structural design and material processing[10-17]. Among them, liquid metal (LM) is one of the best candidates, which possesses ultrahigh stretchability endowed by its intrinsic fluidity. Based on it, various flexible electronic devices are developed including wearable sensors[18,19], capacitors and inductors[20], adjustable rheostats[21], interconnect circuits[22,23], and triboelectric fibers[24].

Recently, encouraging progresses have been made to increase the integration level and robustness of stretchable devices. For example, the jumper wire and multilayer circuits of 3D structure can greatly expand the functionalities of flexible devices and thus their range of applications[25,26]. Although the intrinsic fluidity of LMs at room temperature provides natural stretchability for flexible electronics, however brings difficulties to fabricate 3D structured circuits encapsulated within flexible elastomer. Considerable scientific endeavors have been made for the optimization of fabrication procedures of LM-based devices. Direct writing[27], imprinting[28], laser ablation[29], lithography[22,30], and mechanical/evaporation-induced sintering[31,32] were proposed for 2D wiring and circuit preparation of LMs, but can hardly meet the requirements in 3D circuits. Passivating Ga_2O_3 oxide skin[33,34], freeze solidification[35], and LM composites[36,37] have been developed for the preparation of interconnects within 3D LM circuits, but normally for rather simple 3D structures and cannot be used for large-span and complicated 3D circuits such as those of interconnects or helical structures. The preparation of LM 3D structure circuits both in and out of plane at room temperature is still a great challenge[38]. Moreover, filling LM into pre-constructed microchannels embedded in elastomer using direct injection or vacuum filling

technologies has proven effective for preparing LM electronics featuring customized circuit pattern designs and 3D structure[18,39-43]. However, this widely used method requires a rather complicated preparation process consisting of channel mold fabrication, channel construction, and LM filling. It is technically difficult to prepare long and narrow 3D channels in an elastic polymer. Furthermore, filling LM into such a channel, especially if it features a 3D geometry consisting of curves and/or bends, remains quite troublesome due to the high surface tension of LM which results in poor wetting of the channel surface. Therefore, an easy-to-use and cost-effective method for preparing LM based 3D-structured flexible electronics is urgently needed. The technic paradigm behind above reported methods is to take advantage of the fluidity of LMs. Our hypothesis is that is it possible to make LMs solidified with the plastic property first, manipulated to desired 3D structures, and then return to the liquid state in the final stage (Fig. 1). This will significantly simplify the preparation process. No channels are required and complicated 3D wiring structures can be prepared.

Herein, we report a practical approach to prepare 3D LM flexible electronics without the need for microchannel construction by regulating the alloy composition-dependent material properties of the Ga-In LM alloy. First, we investigate the Ga-10In LM alloy including its phase transition and plastic deformation characteristics. Solidification of LM at low temperatures is utilized to transform the liquid-state bulk Ga-10In alloy into solid-state metallic wires. The excellent plasticity of the solid wire allows the ready formation of rather complex conductive circuit structures using mechanical deformation, bending, or winding. This pre-constructed conductive structure is then directly encapsulated in elastomer and followed by heating to recover its fluidity, thus yielding a stretchable LM conductor for use in flexible electronics. The underlying mechanisms to alloying, phase transition, and plastic deformation using know-how from metallurgy have been systematically investigated using an experimental set-up. We show how this approach can be used rather easily to construct a 2D strain sensor. We also successfully construct an LED array with multiple interconnect arches, a helically-structured finger-wearable device, and a multilayer flexible circuit board, all of them featuring typical 3D-structured circuits. This easy-to-use and cost-effective approach can open new perspectives for the fabrication of LM stretchable electronics.

Results

Strategy of the channel-free method for 3D stretchable conductors

The phase transition and plastic deformation of LM are key factors for the fabrication of LM 3D flexible electronics using our new approach without the need for channel construction. We first optimized the content of In to obtain a good balance between melting point and plasticity in the Ga-10In alloy (Fig. 1a). The differential scanning calorimetry (DSC) analysis of the Ga-10In alloy shows that the Ga-10In alloy starts to melt at 16.3 °C and melting is complete at 22.7 °C (Fig. 1b). Supercooling describes the process of lowering the temperature of a liquid below its freezing point without it becoming a solid until reaching

crystallization temperature. Interestingly, by supercooling the alloy it can remain in a liquid state at temperatures as low as -38 °C. After solidification at -43.6 °C, the Ga-10In alloy completes the transition from a liquid to a solid state and can remain in the solid state even as the temperature is increased again up to ~ 16 °C. A tensile test (Fig. 1c) carried out at 10 °C showed that the Ga-10In alloy possesses a moderate yield strength and excellent elongation which are both crucial for plastic deformation. Ideally, the Ga-10In alloy can be plastically processed after solidification within the solid-state temperature range. In our experiment we used a temperature range of 0 ~ 15 °C.

In our approach, we first induce a liquid-solid phase transition of the Ga-10In alloy via the freeze casting method using silicon tubes with tunable inner diameter as a mold. This allowed us to obtain Ga-10In alloy based solid wires with diameters as small as ~ 60 μm (Fig. S1c, Supporting Information (SI)). These Ga-10In solid wires have a low melting point, moderate strength, excellent plasticity, and can be mechanically processed into any 3D structure as needed for the preparation of 3D-structured stretchable conductors (Fig. 1d). Another key step in the channel-free construction of flexible electronics is the encapsulation process using soft elastomer. We used uncured elastomer to encapsulate the pre-shaped 3D conductive structure after placing it onto a cured elastomer substrate (Fig. 1e). After the two parts of the elastomer have cross-linked to form a single entity, the 3D electronic device is heated to 60 °C to melt the solid Ga-10In wire and regain stretchability (Fig. 1f). Meanwhile, attributing to the supercooling of LM alloy[44], the Ga-10In alloy can remain liquid state at or far below room temperature after melting at high temperature, which ensures that the stretchability of the fabricated devices is maintained across a wide range of applications and usage conditions. The proposed method does not require any microchannel construction, thus eliminating the complicated processes of microchannel mold preparation and troublesome LM filling, while paving the way for the design and manufacture of highly complex 3D circuits.

Quantify and characterize the mechanical and thermal properties of Ga-In alloys

The specific phase transition behavior and mechanical properties of the Ga-In LM alloy, which can be regulated by adjusting the In element content, are crucial to successfully apply our method to the pre-construction of 3D conductive structures. As shown in the Ga-In alloy phase diagram (Fig. S2, SI)[45], in hypoeutectic (In element < 24.5 wt.%)/hypereutectic (In element > 24.5 wt.%) alloys the melting point decreases/increases with increasing In element content. For metals, the content of alloying elements has a significant effect on the overall strength and plasticity of the alloy. Therefore, we synthesized Ga-5In, Ga-10In, and Ga-15In LM alloys (all hypoeutectic) to investigate the influence of In element content on the alloy's microstructure, melting point, and mechanical properties.

Back-scattered electron (BSE) imaging was used to characterize the microstructure of the solid-state Ga-10In alloy (Fig. 2a). Similar to the low-temperature phase separation of LM nanoparticles[46,47], a second phase (A6 phase) is introduced to the matrix with the addition of additional In. The volume fraction of the

A6 phase increases with increasing In element content (Fig. 2b, BSE images of pure Ga, Ga-5In, and Ga-15In are shown in Fig. S3, SI). Energy dispersive X-ray spectroscopy (EDS) element mapping (Fig. S4a, SI) of Ga-10In alloy reveals that the matrix and A6 phase can be clearly distinguished by the element distribution. EDS spot analysis (Fig. S4b, SI) further illustrates that the A6 phase of Spot 1 is a solid solution with Ga atoms dissolved in the In matrix, while there are no In atoms solute in the Ga matrix (Spot 2, A11 phase). The phase composition of Ga-10In and Ga-15In alloys was further investigated by X-ray diffraction (XRD) at a temperature of 0 °C detecting only the α-Ga (PDF-#05-0601) and In phase (PDF-#05-0642) (Fig. 2c). The crystal structures of the two phases are orthorhombic and tetragonal, respectively.

Tensile tests of pure Ga, Ga-5In, Ga-10In, and Ga-15In alloys were conducted at a temperature of 10±3 °C. According to metallurgy theory, dislocation slip is a major mechanism controlling plastic deformation[48,49]. The second phase often tends to hinder dislocation slip thereby increasing alloy strength, a mechanism known as “second phase strengthening”[50,51]. However, stress concentration occurs at the interface between the matrix and second phase and will result in the formation of microcracks that continue to expand into macrocracks and finally cause the interface to be pulled apart. The fracture morphology of the Ga-10In alloy indicates that the microcracks are mainly distributed along the interface between the A6 phase and matrix (Fig. 2d). Hence, the A6 phase is more likely to cause fracture despite increasing alloy strength. The tensile stress-strain curve, yield strength, and elongation *vs.* alloy In element content are shown in Fig. 2e and f. More detailed results of the stress-strain curve and corresponding yield strength, tensile strength, and elongation are provided in Table S1 (SI) which are all consistent with theoretical expectations. Tensile samples of pure Ga, Ga-5In, and Ga-10In after fracture (Fig. S5, SI) exhibit obvious necking and indicate that the fracture mode is plastic fracture. In comparison, the fracture surface of the Ga-15In alloy is flat and presents brittle fracture characteristics. Bending experiments with the Ga-10In and Ga-15In solid wire further verified the superior plasticity of the Ga-10In alloy compared to the Ga-15In alloy (Movie S1, SI). Therefore, Ga-In alloys with an In element content of less than 10 % possess good plastic processing characteristics. Besides, the measured yield strength of below 37.8 MPa requires a relatively low external force to deform the LM alloy, which is convenient for the plastic processing of the Ga-10In solid wire into different conductive structures.

Clearly, the thermal behavior of Ga-In alloys can be significantly influenced by the In element content (Fig. S2, SI). Results from a DSC analysis of pure Ga, Ga-5In, Ga-15In, and Ga-24.5In alloys all showed a peak freezing temperature of about − 40 °C during the cooling cycle (Fig. 2g). However, all these exothermic peaks seem to consist of multiple overlapping peaks suggesting that multiple phase transition processes may be involved[52]. During the heating cycle, pure Ga has an endothermal peak with a melting onset temperature of ~ 30 °C. The endothermic peaks of the Ga-5In, Ga-10In (Fig. 1b), and Ga-15In alloys exhibit bimodal characteristics. From the Ga-In phase diagram (Fig. S2, SI) we can deduce that the left and right exothermic peaks represent the melting processes of the eutectic phase (A6 phase + partial matrix) and remanent matrix, respectively. We consider the temperature at which the matrix melts completely as the melting point and the melting points are summarized in Fig. 2h. Clearly, the melting

point decreases with increasing In element content. We also investigated the dynamics of Ga-10In based wire solidification and melting (Fig. S6, SI) using an optical microscope equipped with a custom-built temperature control system (Fig. S7 and Movie S2, SI). Due to significant supercooling of the LM, the liquid Ga-10In wire does not crystallize when cooled to ~ 0 °C. We therefore introduced a solid LM wire at the right end of the liquid wire to inhibit supercooling and act as a crystallization nucleus which resulted in the liquid wire crystallizing quickly and the solid-liquid interface moving 3.1 mm to the left within a time period of 3 s. On the other hand, the melting process is relatively slow and the non-uniform. The significant supercooling of LM ensures that the Ga-10In alloy remains liquid state across a relatively large range of temperatures keeping stretchable electronics functional even at relatively low temperatures.

The In element content determines the mechanical properties and thermal behavior of the Ga-In alloy as it affects the volume fraction of the eutectic second phase. Compared with the EGaIn alloy with 24.5 wt.% In element content (Ga-24.5In), the lower In element content in our Ga-10In alloy resulted in excellent plasticity and moderate strength. Although the melting point of Ga-10In is slightly higher than EGaIn, the significant supercooling of the Ga-In alloy ensures that the alloy remains in the liquid state for temperatures down to about − 40 °C[44,53]. Therefore, the Ga-10In alloy with its excellent plasticity, low melting point, and moderate strength is the best candidate from among the Ga-In alloys series, to be used in the channel-free construction of 3D flexible electronics.

Before exploring this technique on 3D structured circuits, we first tested our approach to prove the reliability of the channel-free method by fabricating a 2D strain sensor, encapsulating the Ga-10In alloy based LM conductive wires within elastomer and systematically testing the sensor's performance (Fig. 3). Its electromechanical response (Fig. 3a) was similar to previously publish results[54] and the resistance-strain relationship close to theoretical predictions using: $R = R_0(1 + \varepsilon)^2$. However, with increasing strain, some increasing hysteresis appeared in the process of loading and unloading. A previous report[55] suggests that this hysteresis is associated with the channel diameter and may be due to the high flux in narrower channels which causes the relative resistance to fluctuate during the stretching-recovery process. This hysteresis we found in our sensor has also been observed in previous studies of LM strain sensors[55]. Besides, the average gauge factor increases linearly with strain and follows the relationship $\varepsilon + 2$ (Fig. 3b). We found no creep behavior when straining the sensor by up to 80 % in the longitudinal and transverse direction and holding it there for 5 s (Fig. 3c), the absence of creep is crucial for sensing stability. To test for long-term stability, we subjected the sensor to 7500 cycles of 50 % strain and did not find any change in its electromechanical response (Fig. 3d). To demonstrate the strain sensor function, we attached five LM strain sensors on the knuckles of a glove (Fig. 3e), and monitor the motion of the finger in real-time. Signals from five different motions can be obtained and each motion is accurately distinguished (Fig. 3f). The good electromechanical response, long-term stability test, and finger motion detection capability of the 2D strain sensor, all together reflect the high reliability and stability of the device, which demonstrate the practicability and feasibility of further fabricating LM based 3D flexible electronics by the channel-free strategy.

Interconnect Arches For An Integrated Led Array

The cross-arrangement of interconnects has been extensively used in active-matrix displays where 2D structures of transverse and longitudinal interconnects are typically deposited on separate layers to avoid short circuits[34]. 3D interconnects can achieve a cross-arrangement structure on a single plane, avoiding short circuits without requiring separate layers. This can be used to increase the density of interconnects and decrease design complexity, thus allowing the integration of higher density devices in electronic products. Stretchable interconnects can provide an extra degree of freedom for flexible electronic systems while maintaining the same high performance as rigid devices. The Ga-10In solid wire possesses excellent plastic deformability and is therefore easily deformed into a 3D interconnect arch. Figure 4a displays the solid and liquid states of an interconnect arch made of Ga-10In wire on a bending PDMS substrate. Due to the mechanical support provided by the rigid ultrathin Ga_2O_3 film on the surface, the 3D interconnect arch can still maintain its initial status after melting the Ga-10In alloy inside. Simulations of the stress distribution using finite element modeling (FEM) showed that the stress is concentrated near both corners of the arch and is mainly induced by the gravitational weight of the arched area which depends on the radius of curvature (Fig. S8, SI). The bigger the radius of curvature of the arch, the larger its weight and resulting strain on the corner areas, which may lead to the complete collapse of the arch if its weight becomes too large. Based on our experiments, we found that the 3D interconnect arch can persist after melting when the radius of the curvature is less than 3 mm.

For a proof-of-concept demonstration, the interconnect arches were used to construct an LED array (Fig. 4b) with six parallel branches. Three vertical and three horizontal branches cross at right angles using interconnect arches to avoid short circuiting. A specific welding method needs to be developed to resolve the problem of unstable contact between the Ga-10In wire and the LED electrodes (Fig. S9, SI). The stability of the LED array was investigated by bending the array up to radii of curvature of about 20 mm without any visible change in the current-voltage relationship (Fig. 4c). We also found that the current remained constant after bending the array 20,000 times using a 22 mm radius of curvature (Fig. S10, SI), which attests to the long-term stability of the array and Ga-10In interconnect arches. Each branch of our LED array can be independently controlled using a control system composed of a single-chip microcomputer and electric relays (Fig. 4d and e). The timing and sequence for turning the six branches on and off can be controlled by a program (Fig. 4f and Movie S3, SI). These results demonstrate that our interconnect arch is functional and can be used to achieve independent control of the different branches in our example LED array while minimizing the number of interconnections. This method can greatly simplify the circuit designs and reduce manufacturing costs of flexible electronic products.

Wearable Electronic Fingerstall For Remote Monitoring Of Finger Movement

In recent years, considerable attention has been paid to flexible electronics that are deformable and comfortable due to their great potential in wearable electronics[56,57]. However, keeping wearable devices integrated, comfortable and stable has always been a technical difficulty for LM-based wearable electronics. In current work, we further demonstrated a wireless monitoring device that can sense finger movement as shown in Fig. 5a. This device consists of a 3D structured sensor and a module with the function of data processing and wireless transmission. Both 3D structured sensor and multilayer flexible circuit board with voltage stabilizing function are prepared based on the plastic deformation and phase transition mechanisms of the developed Ga-10In, which are very difficult to be prepared using other methods like channel injection.

A technology utilizing the automatic winding machine and Ga-10In solid wire (Fig. S11, SI) was employed to prepare the 3D structured wearable sensor, and the three-step fabrication process is shown in Fig. S12, SI. The wearable sensor (Fig. 5b (i)) consists of a hollow-cylindrical 3D structure with a wall thickness of only 0.94 mm and thus conformably integrates with the finger joints and skin (Fig. S13, SI). This sensor was able to survive tensile tests in the axial (Fig. 5b (ii)) and mechanical squeezing using a tweezer (Fig. 5b (iii)), demonstrating its excellent stretchability and circuit stability which are essential for wearer comfort and sensing stability. The as-designed sensor can quantify the degree of finger bending based on specific changes in its resistance (Fig. 5c), and the normalized resistance change increased with increasing bending angle. Furthermore, $\Delta R/R_0$ remained stable even after 1000 bending cycles using a 32 mm radius of curvature (Fig. 5d), which demonstrates the high level of stability and reliability of this 3D structured wearable sensor. More importantly, the 3D hollow cylinder structured wearable sensor can be directly used as a thermal therapy device to treat the injured joints through thermal expansion of the vascular system and surrounding collagen tissue when applied a direct current. A thermal image shows the effectiveness of this approach in joining the middle joints of the fingers (Fig. S14a, SI), and the heating temperature can be actively adjusted by wearer bend the finger 20 times by a certain angle (Fig. S14b, SI).

The signal measurement of typical wearable sensors mostly uses a rigid circuit board, which would constrain the movement of the human body in certain cases. The miniaturized and integrated flexible circuit board is more comfortable to wear because they are fully attachable to human skin. Here, we prepared a flexible circuit board with 3D wiring in multiple layers, which could conduct voltage regulating function (Fig. S15, SI). The fabrication process is shown in the Fig. S16, SI. The data transmission was accomplished by a Bluetooth module. We employ the Ga-10In solid wires to connect the electronic components including capacitors, resistors, and a voltage regulator (Fig. 5e and Fig. S17, SI), by the welding method explained in Fig. S9, SI. Particularly, the design of “L-shaped” Ga-10In solid wire can connect the circuits in the bottom and top layers (Fig. 5f, g), which provides great convenience for the preparation of the flexible circuit of multilayer as compared to previous work that requires multiple procedures of elastomer cutting and LM filling[23]. We then directly integrated the wearable sensor with the flexible circuit board, and wear them on the finger joints and hand back, respectively (Fig. 5a). The whole device can sensitively distinguish the movement of the finger and wirelessly transmit data to the

computer, achieving remote monitoring of finger movement (Fig. 5h and Movie S6, SI). In contrast to previous works of wearing rigid circuit board on the body[58,59], here the device we developed can closely contact with the skin surface and thus increase the wearing stability and comfortability, which is advantageous merit for the future advancement of wearable electronics.

Discussion

In summary, we successfully demonstrated a channel-free method to fabricate 3D LM based flexible electronics by utilizing the intrinsic phase transition and plastic deformation properties of the Ga-10In LM alloy. By regulating the content of In element, we optimized the alloy composition to provide optimal plasticity, low melting point, and moderate strength. Microstructure analysis suggests that the mechanical properties and thermal behavior of Ga-10In alloy are affected by the amount of A6 phase, which is determined by the In element content in Ga-In alloy. The supercooling effect of the LM alloy allows the Ga-10In alloy to remain in a liquid state even at a temperature far below the melting point which ensures stretchability and normal operation of LM flexible electronics across a relatively broad range of temperatures. To demonstrate the functionality of the as-constructed 3D flexible electronics, we prepared an LED array consisting of multiple independent channels integrated using Ga-10In alloy-based interconnect arches. We further demonstrate a complete set of wearable electronic fingerstall for remote monitoring of finger movement. By making full use of the metallic properties and material performance of the Ga-In alloy, and based on an in-depth understanding of the relation between its microstructure and performance, this approach for manufacturing stretchable 3D conductors opens new perspectives for the design and preparation of LM based flexible electronics. We expect the wide applications of the current method for the fabrication of highly integrated flexible circuit boards, soft human-machine interfaces, and even soft robotics.

Materials And Methods

Materials

Gallium (99.999%) and indium (99.995%) were purchased from Dingguan Metal Technology Co., Ltd (Dongguan City, China). Ga-5In, Ga-10In, Ga-15In (5%, 10%, and 15% In by weight, respectively) alloys were prepared by heating pure Ga and pure In alloys to 190 °C for 1 hour in a vacuum furnace. Before melting, the surface of the In alloy was polished with sandpaper to remove any surface oxide before cleaning it with alcohol. The flexible substrate PDMS (Sylgard 184, Dow Corning) was prepared by mixing the prepolymer and cross-linker at a weight ratio of 10:1. Ecoflex 00–30 (platinum catalyzed silicone elastomer, Smooth-on) was prepared by mixing the two parts at a weight ratio of 1:1. After mixing, the liquid PDMS and Ecolfex 00–30 were placed in a vacuum dryer to remove any bubbles.

Characterization

BSE for microstructure characterization of solid-state alloys was performed at -25 °C using a Phenom Pro scanning electron microscope equipped low-temperature system. Microstructure evolution of the crystallization and melting processes were observed by Leica DM750 microscope equipped with a custom-built heating and cooling system. The phase composition of the Ga-10In and Ga-15In alloys was determined using an XRD diffractometer (X 'Pert Pro MPD) equipped low-temperature system, using a testing temperature and scanning rate of 0 °C and 5° min^{-1}, respectively. Samples with a dimension of 10·10·2 mm for BSE and XRD analysis were cast using a 3D printed mold, frozen to solidification at -70 °C, and then polished in ice water after demolding. The solid-liquid phase change behavior of Ga-In alloys was characterized by DSC (DSC8000, PerkinElmer). Samples with a weight of ~ 40 mg were poured into alumina crucibles with a pipette subjecting them to a cold-heat cycle at a rate of 10 °C min^{-1} under a constant flow of nitrogen of 60 ml min^{-1}.

Performance testing

Low-temperature tensile tests were performed using an AG-250KNI tensile machine with a strain rate of 10^{-3} s^{-1} at 10 °C. Tensile specimens were also prepared using the casting method, and the surface was polished in ice water. The electromechanical response of the 2D strain sensor was tested using a mechanical testing machine (AG-X Plus, Shimadzu) equipped with a resistance meter (Keithley 2010). The wearable sensor tests to detect finger movement was carried out using a Keithley DAQ6510 multi-channel universal meter, while other resistances or voltages of the studied devices were recorded by a Keithley DAQ7510 universal meter.

Fabrication of the LED array

The first layer PDMS was poured into a 60 mm diameter petri dish to a thickness of about 0.5 mm and then cured at 60 °C for 4h. The LEDs were then arranged in an electrode-upward manner on the PDMS according to the design specifications. Then, we encapsulated the second layer of PDMS to the top surface of the LEDs. After curing the second layer of PDMS, we connected the positive and negative poles of the LEDs, distributed in three vertical branches, by straight solid Ga-10In wires with a length of about 11 mm. In order to increase the stability of the connection between the solid wire and the LED electrode, it was necessary to heat both terminals of the straight wire melting about 2 mm at each end. After solidification, the adhesion between the wire and the electrodes was enhanced. Bridge gap interconnects were applied to connect the three horizontal branches in the same way, while the bridge gap structure interconnects were placed at right angles to the straight interconnects. Then, we encapsulated the LED array with a third layer of PDMS and cured for 4h at 60 °C. This PDMS curing caused the Ga-10In solid wire to melt thereby restoring the flexibility of the LED array.

Fabricating and testing the finger wearable 3D sensor

The fabrication process of the 3D wearable sensor is shown in Fig. S12, SI. The first layer of Ecoflex 00–30 silicon was coated onto the surface of the mold with an angular velocity of 1 rad/s, and the thickness was controlled to 0.3 mm by the sheet mold. After the first layer of silicone was cured, the helical coil was

prepared using a moving speed of 18.2 mm/s of the wire feeding platform and an angular speed of 1 rad/s for the mold rotation. Then, we encapsulated the second layer of silicone with a thickness of 0.6 mm in the same way as the first layer of silicon. After curing the silicon, we heated the sensor to 50 °C for 5 minutes and removed it from the mold. The direct current was supplied by a ZhaoXin DSP-6005D using a maximum voltage of 30 V to study the 3D sensor's behavior.

Declarations

Competing interests

The authors declare that they have no competing interests.

References

1. Someya, T. & Amagai, M. Toward a new generation of smart skins. *Nat. Biotechnol.* **37**, 382–388 (2019).
2. Lim, S. et al. Transparent and stretchable interactive human machine interface based on patterned graphene heterostructures. *Adv. Funct. Mater.* **25**, 375–383 (2015).
3. Xie, C., Liu, Jia., Fu, T. Ming., Dai, X., Zhou, W. & Lieber, C. M. Three-dimensional macroporous nanoelectronic networks as minimally invasive brain probes, *Nat. Mater.* **14**, 1286–92(2015).
4. Liu, J. et al. Syringe-injectable electronics, *Nat. Nanotechnol.* **10**, 629–636 (2015).
5. Man, K. & Damasio, A. Homeostasis and soft robotics in the design of feeling machines. *Nat. Mach. Intell.* **1**, 446–452 (2019).
6. Lim, H. R. et al. Advanced soft materials, sensor integrations, and applications of wearable flexible hybrid electronics in healthcare, energy, and environment. *Adv. Mater.* 32, 1901924 (2020).
7. Ling, Y. et al. Disruptive, soft, wearable sensors. *Adv. Mater.* **32**, 1904664 (2020).
8. Chen, S. et al. A Single integrated 3D-printing process customizes elastic and sustainable triboelectric nanogenerators for wearable electronics, *Adv. Func. Mater.* **28**, 1805108 (2018).
9. Guo, Y. et al. Degradable and fully recyclable dynamic thermoset elastomer for 3D-printed wearable electronics, *Adv. Funct. Mater.* **31**, 2009799 (2020).
10. Song, P., Qin, H., Gao, H. L., Cong, H. P. & Yu, S. H. Self-healing and super stretchable conductors from hierarchical nanowire assemblies. *Nat. Commun.* **9**, 2786 (2018).
11. Khang, D. Y., Huang, Y. & Rogers, J. A. A stretchable form of single-crystal silicon for high-performance electronics on rubber substrates. *Science* **311**, 5758 (2006).
12. Fan, J. A. et al. Fractal design concepts for stretchable electronics. *Nat. Commun.* **5**, 3266 (2014).
13. Shyu, T. C. et al. A kirigami approach to engineering elasticity in nanocomposites through patterned defects. *Nat. Mater.* **14**, 785–789 (2015).
14. Liu, Y. et al. Soft and elastic hydrogel-based microelectronics for localized low-voltage neuromodulation. *Nat. Biomed. Eng.* **3**, 58–68 (2019).

15. Wang, Y. et al. A highly stretchable, transparent, and conductive polymer. *Sci. Adv.* **3**, 1602076 (2017).
16. Gao, N., He, Y., Tao, X., Xu, X. Q., Wu,X. & Wang, Y. Crystal-confined freestanding ionic liquids for reconfigurable and repairable electronics. *Nat. Commun.* **10**, 547 (2019).
17. Ma, Z. et al. Permeable superelastic liquid-metal fibre mat enables biocompatible and monolithic stretchable electronics. *Nat. Mater.* 1–10 (2021).
18. Gao, Y. et al. Wearable microfluidic diaphragm pressure sensor for health and tactile touch monitoring. *Adv. Mater.* **29**, 1701985 (2017).
19. Zhou, L. Y., Fu, J. Z., Gao, Q., Zhao, P. & He, Y. All-printed flexible and stretchable electronics with pressing or freezing activatable liquid-metal-silicone inks. *Adv. Funct.* Mater. **30**, 1906683 (2019).
20. Kim, M. G., Alrowais, H., Pavlidis, S. & Brand, O. Size-scalable and high-density liquid-metal-based soft electronic passive components and circuits using soft lithography. *Adv. Funct. Mater.* **27**, 1604466 (2017).
21. Yun, G. et al. Liquid metal composites with anisotropic and unconventional piezoconductivity. *Matter* **3**, 824–841 (2020).
22. Kim, M. G., Brown, D. K. & Brand, O. Nanofabrication for all-soft and high-density electronic devices based on liquid metal. *Nat. Commun.* **11**, 1002 (2020).
23. Liu, S., Shah, D. S. & Kramer-Bottiglio, R. Highly stretchable multilayer electronic circuits using biphasic gallium-indium. *Nat. Mater.* 1–8 (2021).
24. Dong, C. et al. High-efficiency super-elastic liquid metal based triboelectric fibers and textiles. *Nat. Commun.* **11**, 3537 (2020).
25. Marques, D. G., Lopes, P. A., Almeida, A. T. d., Majidib, C. & Tavakoli, M. Reliable interfaces for EGaIn multi-layer stretchable circuits and microelectronics. *Lab Chip* **19**, 897–906 (2019).
26. Hu, J. & Yu, M. F. Meniscus-confined three-dimensional electrodeposition for direct writing of wire bonds. *Science* **329**, 313–316 (2010).
27. Boley, J. W., White, E. L., Chiu, G. T. C. & Kramer, R. K. Direct writing of gallium-indium alloy for stretchable electronics. *Adv. Funct. Mater.* **24**, 3501–3507 (2014).
28. Park, J. E., Kang, H. S., Koo, M. & Park, C. Autonomous surface reconciliation of a liquid-metal conductor micropatterned on a deformable hydrogel. *Adv. Mater.* **32**, 2002178 (2020).
29. Pan, C., Kumar, K., Li, J., Markvicka, E. J., Herman, P. R. & Majidi, C. Visually imperceptible liquid-metal circuits for transparent, Stretchable electronics with direct laser writing. *Adv. Mater.* **30**, 1706937 (2018).
30. Gozen, B. A., Tabatabai, A., Ozdoganlar, O. B. & Majidi, C. High-density soft-matter electronics with micron-scale line width. *Adv. Mater.* **26**, 5211–5216 (2014).
31. Boley, J. W., White, E. L. & Kramer, R. K. Mechanically sintered gallium-indium nanoparticles. *Adv. Mater.* **27**, 2355–2360 (2015).
32. Li, X., Li, M., Xu, J., You, J., Yang, Z. & Li, C. Evaporation-induced sintering of liquid metal droplets with biological nanofibrils for flexible conductivity and responsive actuation. *Nat. Commun.* **10**, 3514

(2019).

33. Ladd, C., So, J. H., Muth, J. & Dickey, M. D. 3D printing of free standing liquid metal microstructures. *Adv. Mater.* **25**, 5081–5085 (2013).
34. Park, Y.-G., An, H. S., Kim, J. Y. & Park, J. U. High-resolution, reconfigurable printing of liquid metals with three-dimensional structures. *Sci. Adv.* **5**, 2844 (2019).
35. Gannarapu, A. & Gozen, B. A. Freeze-printing of liquid metal alloys for manufacturing of 3D, conductive, and flexible networks. *Adv. Mater. Technol.* **1**, 1600047 (2016).
36. Park, Y. G., Min, H., Kim, H., Zhexembekova, A., Lee, C. Y. & Park, J. U. Three-dimensional, high-resolution printing of carbon nanotube/liquid metal composites with mechanical and electrical reinforcement. *Nano. Lett.* **19**, 4866–4872 (2019).
37. Votzke, C., Daalkhaijav, U., Menguc, Y. & Johnston, M. L. 3D-printed liquid metal interconnects for stretchable electronics. *IEEE Sens. J.* **19**, 3832–3840 (2019).
38. Yu, Y., Liu, F., Zhang, R. & Liu, J. Suspension 3D printing of liquid metal into self-healing hydrogel, *Adv. Mater. Technol.* **2**, 1700173 (2017).
39. Bharambea, V., Parekhb, D. P., Laddb, C., Moussac, K., Dickeyb, M. D. & Adams, J. J. Vacuum-filling of liquid metals for 3D printed RF antennas. *Addit. Manuf.* **18**, 221–227 (2017).
40. Teng, L., Ye, S., Wang, S. H., Zhou, X., Gan, T. & Zhou, X. Liquid metal-based transient circuits for flexible and recyclable electronics. *Adv. Funct. Mater.* **29**, 1808739 (2019).
41. Yeo, J. C., Yu, J., Koh, Z. M., Wang, Z. & Lim, C. T. Wearable tactile sensor based on flexible microfluidics. *Lab. Chip.* **16**, 3244–3250 (2016).
42. Cooper, C. B. et al. Stretchable capacitive sensors of torsion, strain, and touch using double helix liquid metal fibers. *Adv. Funct. Mater.* **27**, 1605630 (2017).
43. Kim, K. et al. Highly sensitive and wearable liquid metal-based pressure sensor for health monitoring applications: integration of a 3D-printed microbump array with the microchannel. *Adv. Healthc. Mater.* **8**, 1900978 (2019).
44. Malakooti, M. H., et al. Liquid metal supercooling for low-temperature thermoelectric wearables. *Adv. Funct. Mater.* **29**, 1906098 (2019).
45. Aderson, T. J. & Ansara, I. The Ga-In (Gallium-Indium) system. *J. Phase Equilib.* **12**, 64–72 (1991).
46. Ren, L. et al. Nanodroplets for stretchable superconducting circuits. *Adv. Funct. Mater.* **26**, 8111–8118 (2016).
47. Tang, S. Y. et al. Phase separation in liquid metal nanoparticles. *Matter* **1**, 192–204 (2019).
48. Wu, Z. X., Zhang, Y. W. & Srolovitz, D. J. Dislocation-twin interaction mechanisms for ultrahigh strength and ductility in nanotwinned metals. *Acta Mater.* **57**, 4508–4518 (2009).
49. Zhang, Z. et al. Dislocation mechanisms and 3D twin architectures generate exceptional strength-ductility-toughness combination in CrCoNi medium-entropy alloy. *Nat. Commun.* **8**, 14390 (2017).
50. Matsukawa, Y. et al. The effect of crystallographic mismatch on the obstacle strength of second phase precipitate particles in dispersion strengthening: bcc Nb particles and nanometric Nb clusters

embedded in hcp Zr. *Acta Mater.* **102**, 323–332 (2016).

51. Tang, S. et al. Precipitation strengthening in an ultralight magnesium alloy. *Nat. Commun.* **10**, 1003 (2019).
52. Wolny, J., Nizioł, S., Łużny, W., Pytlik, L., Sołtys, J. & Kokoszka, R. Structure changes in gallium near its melting point. *Solid State Commun.* **58**, 573–575 (1986).
53. Bautista, R. G. Gallium Metal Recovery. *J. Miner. Met. Mater. Soc.* **41**, 30–31 (1989).
54. Jin, Y., Lin, Y., Kiani, A., Joshipura, I. D. Ge, M. & Dickey, M. D. Materials tactile logic via innervated soft thermochromic elastomers. *Nat. Commun.* **10**, 4187 (2019).
55. Wu, Y. et al. Liquid metal fiber composed of a tubular channel as a high-performance strain sensor. *J. Mater. Chem. C* **5**, 12483–12491 (2017).
56. Wang, C., Xia, K., Wang, H., Liang, X., Yin, Z. & Zhan, Y. Advanced carbon for flexible and wearable electronics. *Adv. Mater. 31*, 1801072 (2019).
57. Wang, X., Liu, Z. & Zhang, T. Flexible sensing electronics for wearable/attachable health monitoring. *Small 13*, 1602790 (2017).
58. Liu, Z. et al. Surface Strain redistribution on structured microfibers to enhance sensitivity of fiber-shaped stretchable strain sensors, *Adv. Mater. 30*, 1704229(2018).
59. Bartlett, M. D., Markvicka, E. J. & Majidi, C. Rapid fabrication of soft, multilayered electronics for wearable biomonitoring, *Adv. Funct. Mater. 26*, 8496–8504 (2016).

Figures

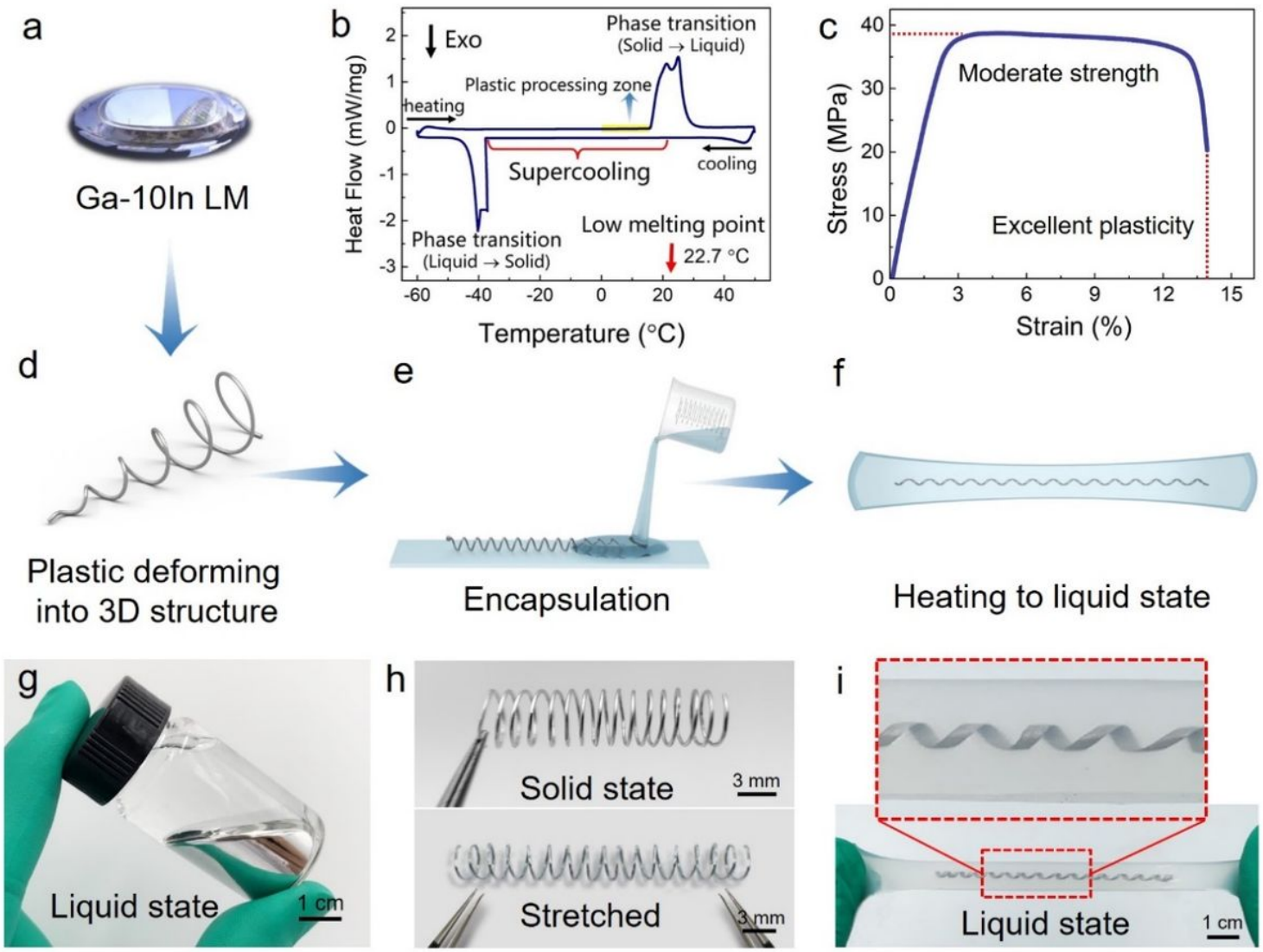

Figure 1

Using phase transitions and plastic deformation of the Ga-10In LM alloy allows for a channel-free construction of 3D stretchable conductors. a) The Ga-10In alloy with excellent plasticity, moderate strength, and low melting point. b) Differential scanning calorimetry (DSC) heat flux as a function of temperature for the Ga-10In LM alloy. The solidified Ga-10In alloy is deformed into multiple conductive structures and encapsulated by the polymer in the plastic processing zone. After being heated to melt, it can remain in a liquid state down to about -40 °C due to supercooling. c) The tensile stress-strain curve of the Ga-10In alloy tested at 10 °C while in solid state. The elongation of up to 14 % proves that Ga-10In possesses excellent plasticity. d) The Ga-10In solid wire can be deformed into any 3D conductive structure including helical. e) The encapsulation process by polymer-based elastomer. f) The device is heated to 60 °C to induce melting of the solid Ga-10In solid wire and thereby restore stretchability. g) Photograph of liquid-state Ga-10In alloy. h) The helical structure of Ga-10In solid wire before (top) and after (below) being stretched. i) Photograph of the 3D stretchable device, and enlarged picture shows the liquid-state Ga-10In circuit with 3D helical structure encapsulated in the polymer.

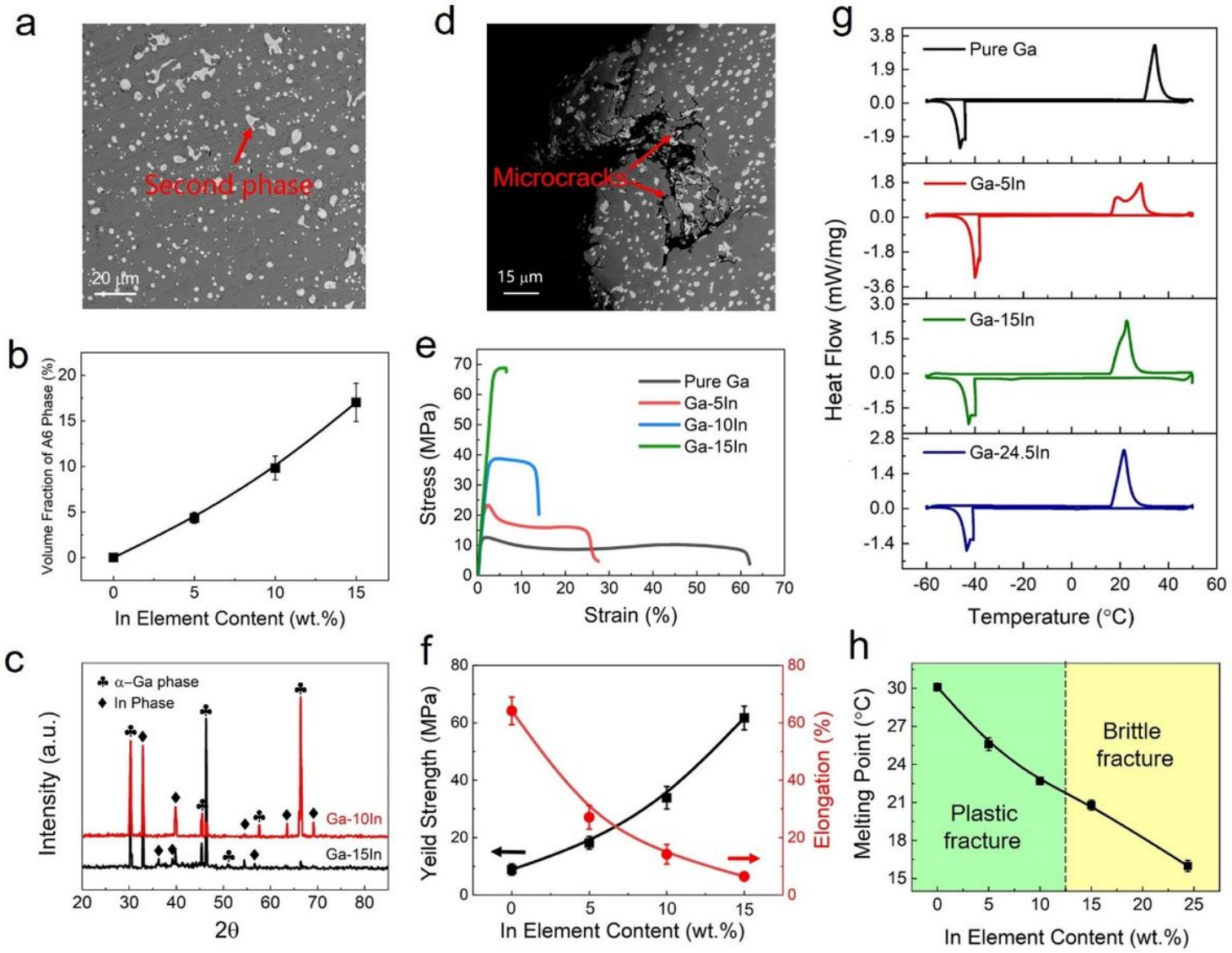

Figure 2

Microstructure characterization and performance test of the different Ga-In alloys. a) BSE image taken at -20 °C showing the distribution and content of the A6 phase in the Ga-10In alloy. Adding In to the Ga-In alloy will introduce the A6 phase through the phase separation process. b) Volume fraction of the A6 phase in pure Ga, Ga-5In, Ga-10In, and Ga-15In alloys, estimated from its area fraction in BSE images. c) XRD characterization of Ga-10In and Ga-15In alloys proving that the A6 phase in (a) is In rich. d) Fractograph of the Ga-10In alloy after a low temperature tensile test; the microcracks are mainly distributed along the phase interface indicating that A6 phases are likely to cause the initial development and subsequent propagation of cracks. e) Low temperature tensile stress-strain curve of pure Ga, Ga-5In, Ga-10In, and Ga-15In alloys. f) Tensile yield strength and elongation for the alloys shown in (e). g) Normalized DSC heat flux as a function of temperature for pure Ga, Ga-5In, Ga-15In, and Ga-24.5In alloys. h) Melting points measured by DSC analysis of the different Ga-In alloys. The melting point decreases with increasing In content. When the In element content is higher than about 10~15 wt.%, the alloy exhibits brittle fracture in the solid state.

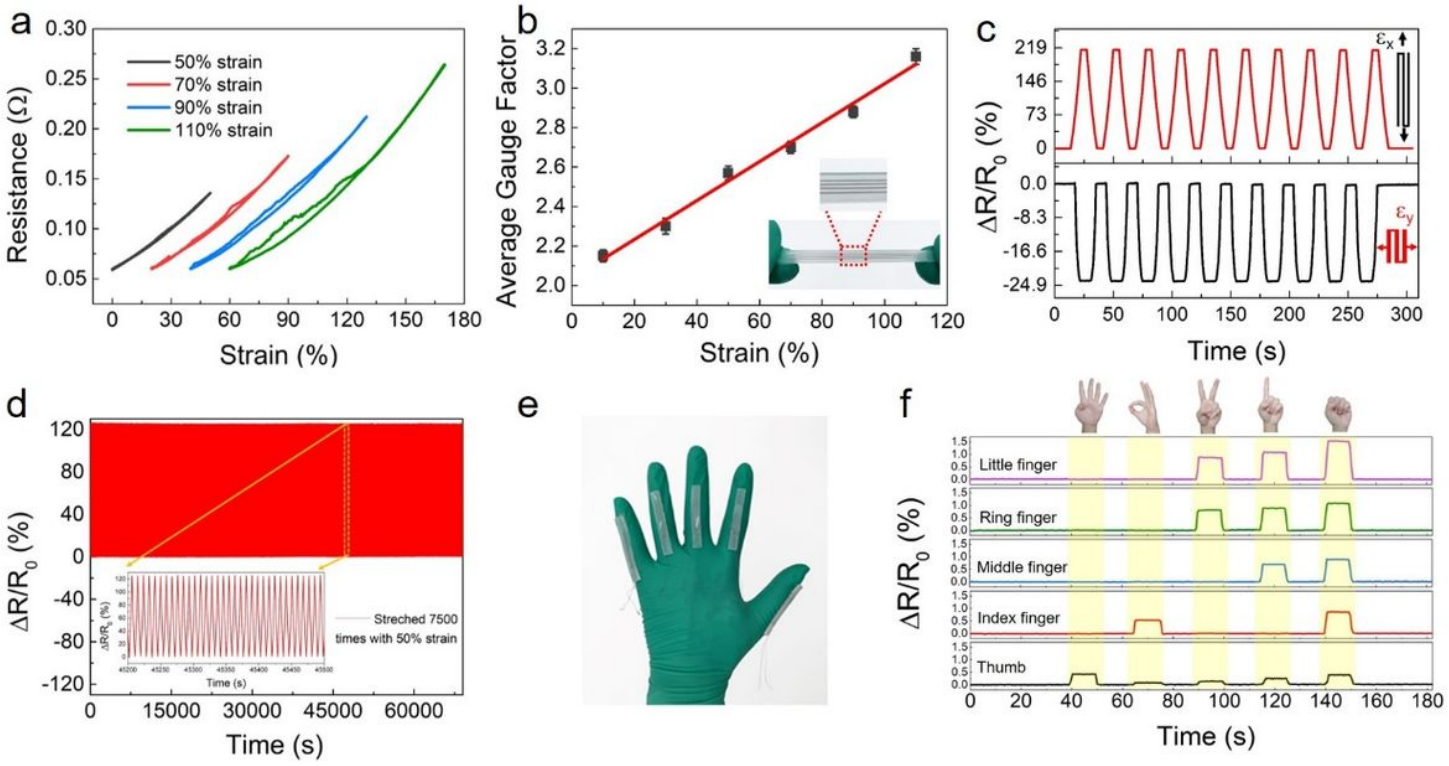

Figure 3

Electromechanical tests performed on the channel-free-constructed 2D strain sensor and its application for monitoring finger movement. a) Electromechanical response of the strain sensor as a function of strain. b) Average gauge factor as a function of strain; the inset shows a photograph of the channel-free-constructed 2D LM strain sensor in stretched state. c) Electromechanical response of the sample when strained to 80 % in the longitudinal and transverse direction and held for 5 s at each half-cycle. d) Testing the sensor long-term stability by subjecting it to 7500 tensile cycles with 50 % strain. The inset shows a zoom of a representative time interval demonstrating the stability of the relative resistance over time. e) Photograph showing the strain sensor mounted onto a wearable glove. f) Motion detection of finger bending and straightening while performing different hand gestures; the five lines correspond to the five fingers from little finger (top) to thumb (bottom).

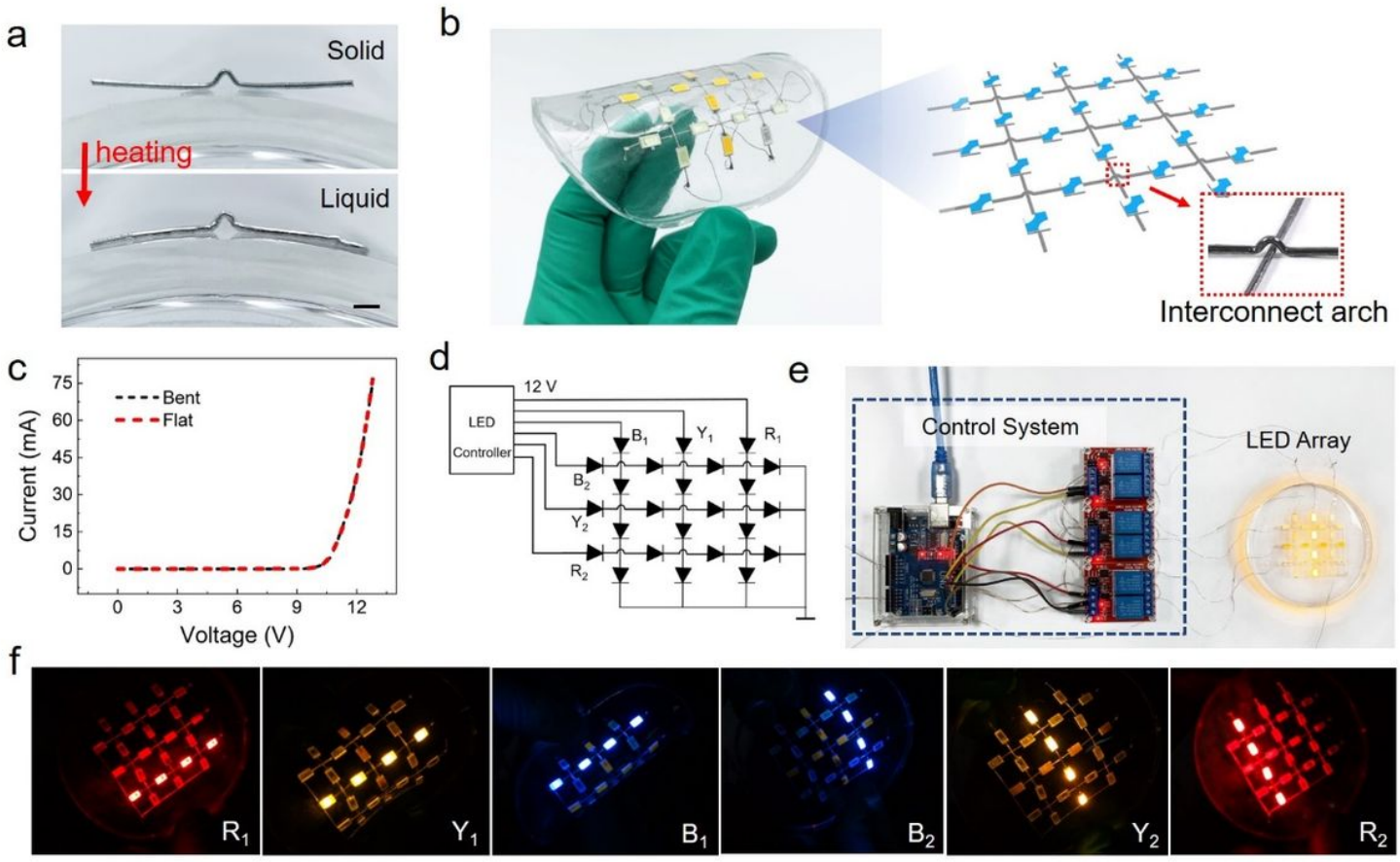

Figure 4

Ga-10In 3D interconnect arch and its use in an LED array. a) Photographs of an interconnect arch in solid and liquid states on a bending PDMS substrate; the scar bar corresponds to 1 mm. The arch structure can maintain its initial state after melting due to the rigid oxide “skin” of the Ga2O3 nanolayer on the surface. b) Photograph of the flexible LED array consisting of multiple 3D interconnect arches. A simple circuit structure is sufficient to prevent short circuits. c) Current-Voltage characteristics of the LED array when bent (radius of curvature about 20 mm) and while flat demonstrating the high stability of the interconnect arches. d) Circuit diagram of the control system and LED array to achieve independent control of the six branches; B, Y, and R represent the LED colors blue, yellow, and red, respectively. e) Photograph of the control system and LED array. f) Photographs of the LED array when each of the six branches was switched on independently.

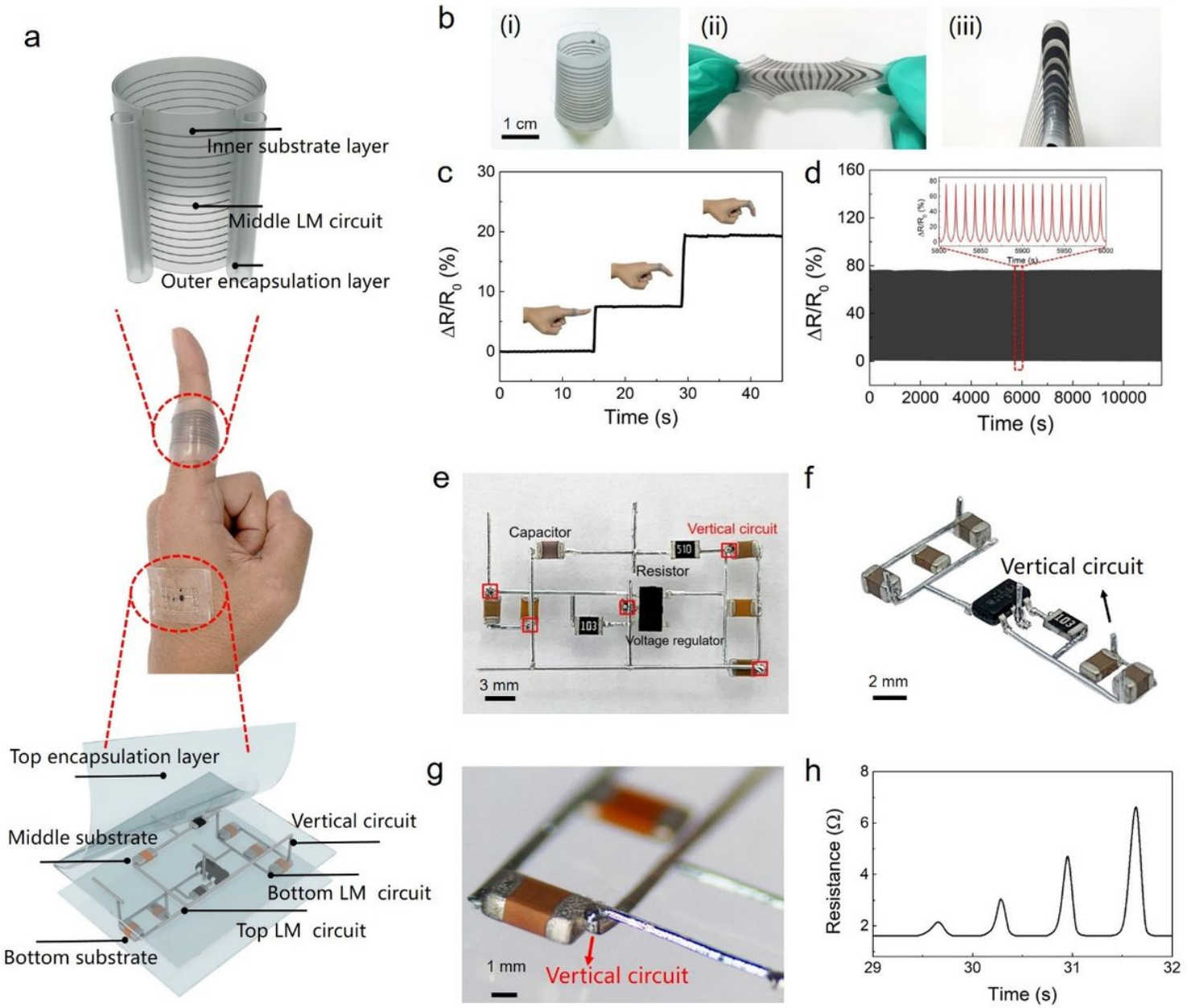

Figure 5

Design and fabrication of 3D structured wearable finger movement detection sensor and multilayer flexible circuit board using Ga-10In solid wire. a) The models of 3D structured wearable sensor and flexible circuit board wearing on finger and back of the hand, respectively. b) Photograph of the 3D structured wearable sensor and demonstration of its good stretchability under tensile and squeeze tests. This kind of structure would be very difficult to prepare using injection or other methods. c) Response of the wearable sensor to different finger curvatures. d) ΔR/R0 during 1000 cycles of bending using a 32 mm radius of curvature demonstrating its high long-term stability. e) Top view of the flexible circuit board with voltage stabilizing function. f) Photograph of the first layer circuit and components. g) The vertical circuit that connect the circuits of the first and second layer. h) The typical raw data obtained by the

wearable sensor and transmitted utilizing wireless signal processing device when monitoring the process of finger bending and straightening.

Supplementary Files

This is a list of supplementary files associated with this preprint. Click to download.

- SupplementaryInformation.docx
- MovieS1.mp4
- MovieS2.mp4
- MovieS3.mp4
- MovieS4.mp4
- MovieS5.mp4
- MovieS6.mp4